# PRECISE MEASUREMENT OF COSMIC-RAY PROTON AND HELIUM SPECTRA WITH THE BESS SPECTROMETER

T. SANUKI,[1] M. MOTOKI,[1,2] H. MATSUMOTO,[1] E. S. SEO,[3] J. Z. WANG,[3] K. ABE,[1] K. ANRAKU,[1] Y. ASAOKA,[1]
M. FUJIKAWA,[1] M. IMORI,[1] T. MAENO,[4] Y. MAKIDA,[5] N. MATSUI,[1] H. MATSUNAGA,[1,6] J. MITCHELL,[7]
T. MITSUI,[2,4] A. MOISEEV,[7] J. NISHIMURA,[1] M. NOZAKI,[4] S. ORITO,[1] J. ORMES,[7] T. SAEKI,[1]
M. SASAKI,[5] Y. SHIKAZE,[1] T. SONODA,[1] R. STREITMATTER,[7] J. SUZUKI,[5] K. TANAKA,[5]
I. UEDA,[1] N. YAJIMA,[8] T. YAMAGAMI,[8] A. YAMAMOTO,[5]
T. YOSHIDA,[5] AND K. YOSHIMURA[1]

## ABSTRACT

We report cosmic-ray proton and helium spectra in energy ranges of 1–120 GeV nucleon$^{-1}$ and 1–54 GeV nucleon$^{-1}$, respectively, measured by a flight of the Balloon-borne Experiment with Superconducting Spectrometer (BESS) in 1998. The magnetic rigidity of the cosmic ray was reliably determined by highly precise measurement of the circular track in a uniform solenoidal magnetic field of 1 T. Those spectra were determined within overall uncertainties of $\pm 5\%$ for protons and $\pm 10\%$ for helium nuclei including statistical and systematic errors.

*Subject headings:* cosmic rays — elementary particles

## 1. INTRODUCTION

The absolute fluxes and spectra of primary cosmic-ray protons and helium nuclei are fundamental information as references in cosmic-ray physics. They are needed to calculate secondary antiprotons, positrons, and diffuse gamma radiation, which in turn provide important knowledge of particle propagation and matter distribution in the interstellar space. Those are also indispensable for studying atmospheric neutrinos. Although measurement of the proton and helium energy spectra has been performed in various experiments, their resultant absolute fluxes show discrepancies up to a factor of 2 at 50 GeV nucleon$^{-1}$. This ambiguity causes large uncertainties in calculations of the atmospheric neutrinos, as well as secondary antiprotons, positrons, and diffuse gamma rays.

We report a new precise measurement of the cosmic-ray proton and helium spectra focused on energy ranges of 1–120 GeV nucleon$^{-1}$ for protons and 1–54 GeV nucleon$^{-1}$ for helium nuclei, based on half of the data from a Balloon-borne Experiment with Superconducting Spectrometer (BESS) flight in 1998. The covered energy range is relevant to the atmospheric neutrinos observed as "fully contained events" in Super-Kamiokande (Fukuda et al. 1998). These spectra are also significant for other neutrino experiments such as MACRO (Ambrosio et al. 1998) and SOUDAN-2 (Allison et al. 1999). In the BESS-98 flight, a new trigger mode was implemented with a silica aerogel Cerenkov counter to record all energetic particles instead of sampling the protons at a ratio of 1/60 as done in the previous BESS flights. This drastically improved statistics in the high-energy region above 6 GeV nucleon$^{-1}$, as reported here.

In accordance with a variation of solar activity, a change of the proton and helium spectra in the low-energy range has been observed since the first flight of the BESS in 1993. Further detailed analysis of the solar modulation affecting the low-energy spectra in a series of BESS flight experiments will be discussed elsewhere.

## 2. THE BESS SPECTROMETER

The BESS detector is a high-resolution spectrometer with a large acceptance to perform highly sensitive searches for rare cosmic-ray components, as well as precise measurement of the absolute fluxes of various cosmic-ray particles (Orito 1987; Yamamoto et al. 1994; Ajima et al. 2000). As shown in Figure 1, all detector components are arranged in a simple cylindrical configuration with a thin superconducting solenoidal magnet.

In the central region, the solenoid provides a uniform magnetic field of 1 T. The field deviation is less than 2.5% along a typical trajectory of an incoming particle. The trajectory is measured by a tracking system which consists of a central jet-type drift chamber (JET) chamber and two inner drift chambers. A volume of the tracking system is 0.84 m in diameter and 1 m in length. The magnetic rigidity ($R \equiv pc/Ze$) is reliably determined by applying a simple circular fitting to the trajectory. The deflection ($R^{-1}$) and its error ($\Delta R^{-1}$) are calculated for each event by a fitting method by Karimäki (1991) using up to 28 hit points each with a spatial resolution of 200 $\mu$m. Figure 2 shows a distribution of the deflection resolution for protons evaluated in the track-fitting procedure together with those of other spectrometers used in previous balloon experiments (Boezio et al. 1999; Menn et al. 2000). Each area of the histogram is normalized to unity. The peak position of 0.005 GV$^{-1}$ corresponds to a maximum detectable rigidity (MDR) of 200 GV. Since the magnetic field is highly uniform, it has a narrow and sharp peak with a small tail. This means the accuracy of rigidity measurement has been improved in comparison with previous balloon experiments.

[1] Postal address: University of Tokyo, Bunkyo, Tokyo 113-0033, Japan; sanuki@phys.s.u-tokyo.ac.jp.
[2] Currently at Tohoku University, Sendai, Miyagi 980-8578, Japan.
[3] University of Maryland, College Park, MD 20742.
[4] Kobe University, Kobe, Hyogo 657-8501, Japan.
[5] High Energy Accelerator Research Organization (KEK), Tsukuba, Ibaraki 305-0801, Japan.
[6] Currently at University of Tsukuba, Tsukuba, Ibaraki 305-8571, Japan.
[7] NASA Goddard Space Flight Center, Greenbelt, MD 20771.
[8] The Institute of Space and Astronautical Science, Sagamihara, Kanagawa 229-8510, Japan.
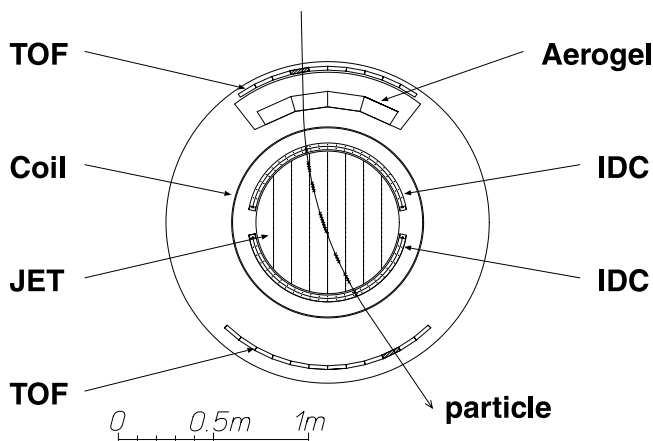
FIG. 1.—Cross-sectional view of the BESS instrument

The outermost detector is a set of time-of-flight (TOF) hodoscopes (Shikaze et al. 2000). Their top and bottom layers are segmented into 10 and 12 paddles, respectively, each of which has a $95 \times 10 \times 2$ cm$^3$ plastic scintillator. It provides the velocity ($\beta \equiv v/c$) and energy loss ($dE/dx$) measurements. The time resolution for energetic protons in each counter was 55 ps rms, resulting in a $\beta^{-1}$ resolution of 1.4%. The data acquisition sequence is initiated by a first-level TOF trigger, which is a simple coincidence of signals in the top and bottom scintillators with the threshold level of $\frac{1}{3}$ pulse height from minimum ionizing particles (MIPs). If the pulse height exceeds 2.5 times the MIP signal, the TOF trigger is labeled as "helium trigger," otherwise "proton trigger." In order to build a sample of unbiased triggers, 1 of every 60 "proton-triggered" and 1 of 25 "helium-triggered" events were recorded irrespective of succeeding on-line selections, which enriched negatively charged particles such as antiprotons (Ajima et al. 2000). The TOF trigger efficiency was estimated to be about 99.9% by examining measured $dE/dx$ distributions and the threshold level. It was cross-checked by using the secondary beam at the KEK[9] 12 GeV proton synchrotron. The TOF trigger efficiency was evaluated to be 99.4% $\pm$ 0.2% for 1.67 GeV $c^{-1}$ protons and antiprotons, whose energy loss rate is

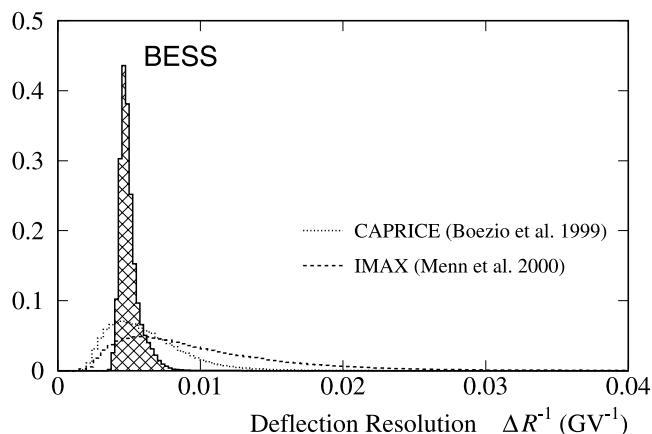[9] High Energy Accelerator Research Organization, Japan.



FIG. 2.—Distribution of the deflection resolution for protons evaluated for each event in the track-fitting procedure. Each area of the histogram is normalized to unity.

1.3 times higher than MIPs. The inefficiency of 0.6% is mainly due to a geometrical inefficiency caused by gaps between scintillator paddles. It was independently estimated to be 0.6% from a Monte Carlo simulation of the BESS detector. Thus, the systematic error caused by the TOF trigger inefficiency is negligibly small.

The instrument has a threshold-type Cerenkov counter with a silica aerogel radiator just below the top TOF hodoscope (Asaoka et al. 1998). The radiator was newly developed prior to the BESS-98 flight, and it has a refractive index of 1.020 (Sumiyoshi et al. 1998). In addition to the TOF trigger, an auxiliary trigger is generated by a signal from the Cerenkov counter to record energetic particles without bias or sampling. The efficiency of the Cerenkov trigger and its energy dependence were evaluated as a ratio of the Cerenkov-triggered events among the unbiased trigger sample. It was about 70% at 6 and 4 GeV nucleon$^{-1}$ for protons and helium nuclei, respectively, and smoothly increased with energy. The efficiency for relativistic particles ($R > 20$ GV, $\beta \to 1$) was 92.1% $\pm$ 3.0%. The accuracy of the efficiency was limited by statistics of the unbiased trigger sample.

Below 6.31 GeV nucleon$^{-1}$ for protons and 3.98 GeV nucleon$^{-1}$ for helium nuclei, only the TOF-triggered events were analyzed to obtain the energy spectra. The Cerenkov-triggered events were also used in addition to TOF-triggered events in higher energy regions, where much better statistics were achieved as described in § 5.

The BESS spectrometer was flown from Lynn Lake, Manitoba, Canada, 1998 July 29–30. It floated at an altitude of 37 km (residual atmosphere of 5 g cm$^{-2}$) with a cutoff rigidity of 0.5 GV or smaller. The solar activity was close to the minimum.

## 3. DATA ANALYSIS

### 3.1. Data Reduction

In the first stage of data reduction, we selected events with a single track fully contained inside the fiducial volume defined by the central four columns out of eight columns in the JET chamber. This definition of the fiducial volume reduced the effective geometrical acceptance down to $\sim\frac{1}{3}$ of the full acceptance, but it ensured the longest track fitting and thus the highest resolution in the rigidity measurement. A single-track event was defined as an event which has only one isolated track and one or two hit counters in each layer of the TOF hodoscopes. The single-track selection eliminated rare interacting events. In order to verify the selection, events were scanned randomly in the unbiased trigger sample, and it was confirmed that 995 out of 1000 visually identified single-track events passed this selection criteria, and interacting events were fully eliminated. Thus, the track reconstruction efficiency was estimated to be 99.5% $\pm$ 0.2% for a single-track event. The single-track events selected in this stage underwent a succeeding analysis.

Particle identification was performed as shown in Figure 3 by requiring proper $dE/dx$ and $1/\beta$ as functions of rigidity. A pair of solid lines in each graph defines a proton band, and superimposed graphs show proton selection criteria above 10 GV. Helium nuclei were selected in the same manner. Figure 3a shows the proton selection band in a $dE/dx$ inside the top TOF scintillators versus rigidity plane, which selected singly charged particles. A $dE/dx$ in the bottom TOF was also examined. In order to estimate effi-
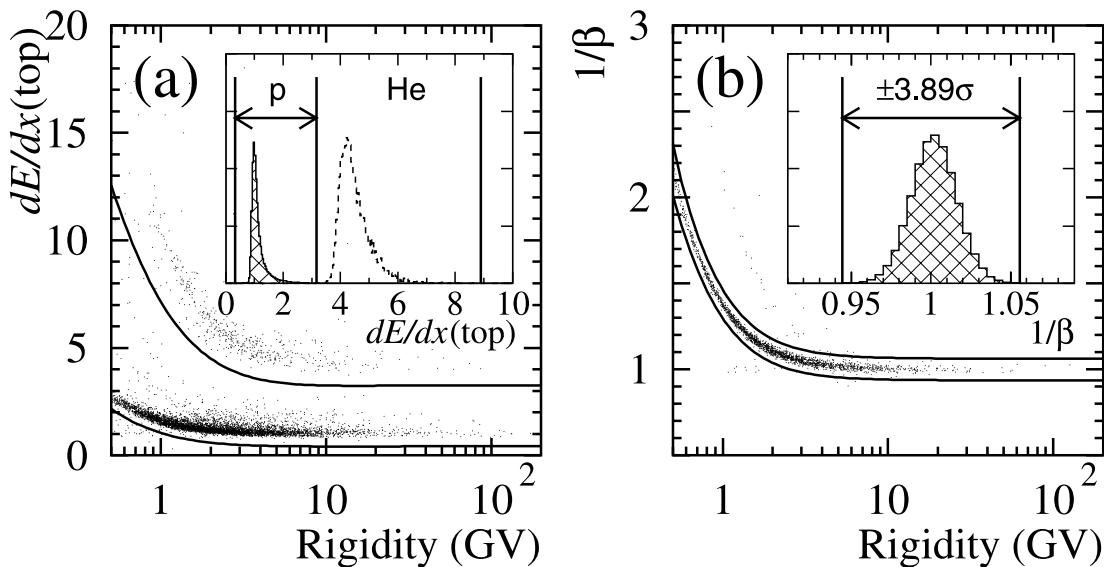
FIG. 3.—Proton bands in (a) $dE/dx$ (top TOF) vs. rigidity plane and (b) $1/\beta$ vs. rigidity plane after proton $dE/dx$ selection. A $dE/dx$ in the bottom TOF was also checked. The superimposed graphs show the proton selection criteria above 10 GV. Helium nuclei were selected in the same manner.

ciencies and contamination probabilities, another sample of $5 \times 10^5$ protons and $4 \times 10^4$ helium nuclei were selected by using independent information of energy loss inside the JET chamber. According to a study of the sample, it was found that $99.3\% \pm 0.2\%$ of protons and $98.2\% \pm 0.7\%$ of helium nuclei were properly identified by the $dE/dx$ selection and that the contamination probabilities should be less than $3 \times 10^{-5}$ for protons and $4 \times 10^{-4}$ for helium nuclei. The errors of the efficiencies arose from limited statistics of the sample. After the $dE/dx$ selection, an appropriate relationship between $1/\beta$ and rigidity was required as shown in Figure 3b. Since the $1/\beta$ distribution is well described by Gaussian and a half-width of the $1/\beta$ selection band was set at 3.89 $\sigma$, the efficiency is very close to unity (99.99% for pure Gaussian).

Very clean proton samples were obtained below 2 GV. As shown in Figure 3b, however, light particles, such as positrons and muons, started to contaminate the proton band at around 2 GV and deuterons at around 3 GV where the deuteron contamination was observed to be 2%. It was found that the ratio of observed light particles to protons was about 10% at 0.4 GV and rapidly dropped to 0.8% at 2 GV; thus, deuterons were the main contamination in the proton band above 1 GeV nucleon$^{-1}$. No subtraction was made for the deuteron contamination because it was as small as the statistical errors and a deuteron-to-proton ratio decreases with increasing energy (Seo et al. 1997) following a decrease in escape path lengths of primary cosmic-ray nuclei (Engelmann et al. 1990). Therefore, above 3 GV hydrogen nuclei were selected, which included a small amount of deuterons. In conformity with previous experiments, all doubly charged particles were treated as $^4$He.

In order to assure accuracy of the rigidity measurement, event qualities such as $\chi^2$ in the track-fitting procedure were imposed on the single-track events after the particle identification. The efficiency of this quality check was evaluated to be $93.8\% \pm 0.3\%$ for protons and $93.0\% \pm 0.9\%$ for helium nuclei as a ratio of the number of good quality events to all events between 10 and 20 GeV nucleon$^{-1}$. Since the quality check required consistency between each hit in the tracking

detector and the fitted track, it could be reasonably assumed and has been confirmed in the analysis that its efficiency does not depend on energy in the higher energy region where multiple scattering can be neglected. Accordingly, the above values of quality check efficiency were applied to the higher energy region. Before and after the quality check and succeeding correction of its efficiency, the obtained proton and helium fluxes above 10 GeV nucleon$^{-1}$ changed no more than $\pm 0.3\%$ and $\pm 0.9\%$, respectively. These changes were treated as systematic errors in the quality check. Below 10 GeV nucleon$^{-1}$, quality check was not imposed because rigidity resolution before the quality check was high enough to measure the energy. Thus, there is no systematic error associated with the quality check.

With the data reduction described above, 826,703 protons and 77,325 helium nuclei were finally identified. The combined efficiencies in the data reduction process were $98.8\% \pm 0.3\%$ and $97.7\% \pm 0.8\%$ for TOF-triggered proton and helium samples, respectively. For Cerenkov-triggered samples above 10 GV, the combined efficiency was $92.7\% \pm 0.4\%$ for protons and $90.8\% \pm 1.2\%$ for helium nuclei.

### 3.2. Normalization and Corrections

In order to determine the primary cosmic-ray proton and helium spectra at the top of the atmosphere, the following normalization and corrections are required: (1) exposure factor, (2) ionization energy loss, (3) interaction loss, and (4) atmospheric secondary particle contribution.

The exposure factor is a product of geometrical acceptance and live time. The geometrical acceptance defined for this analysis was calculated by simulation technique (Sullivan 1971) to be $0.0851 \pm 0.0003$ m$^2$ sr for energetic particles which have straight track inside the tracking volume. It was almost constant over the whole energy range. The simple cylindrical shape and the uniform magnetic field make it simple and reliable to determine the geometrical acceptance precisely. The error arose from uncertainty of the detector alignment within 1 mm. The live

TABLE 1

SELECTION EFFICIENCIES (%) AT EACH STEP

| | PROTON KINETIC ENERGY (GeV nucleon$^{-1}$) | | | HELIUM KINETIC ENERGY (GeV nucleon$^{-1}$) | |
| --- | --- | --- | --- | --- | --- |
| SELECTION CRITERIA | 1 | 10 | 100 | 1 | 10 |
| Trigger ..................... | $(100)^{a}$ | $88.5 \pm 3.0$ | $92.1 \pm 3.0$ | $(100)^{a}$ | $92.1 \pm 3.0$ |
| Track reconstruction ...... | $99.5 \pm 0.2$ | $99.5 \pm 0.2$ | $99.5 \pm 0.2$ | $99.5 \pm 0.2$ | $99.5 \pm 0.2$ |
| Particle identification...... | $99.3 \pm 0.2$ | $99.3 \pm 0.2$ | $99.3 \pm 0.2$ | $98.2 \pm 0.7$ | $98.2 \pm 0.7$ |
| Event quality ............... | $(100)^{b}$ | $93.8 \pm 0.3$ | $93.8 \pm 0.3$ | $(100)^{b}$ | $93.0 \pm 0.9$ |
| Penetrate the BESS........ | $87.6 \pm 2.3$ | $82.3 \pm 2.7$ | $79.7 \pm 2.9$ | $74.5 \pm 6.9$ | $68.5 \pm 7.2$ |

[a] Below 6.31 GeV nucleon$^{-1}$ for protons and 3.98 GeV nucleon$^{-1}$ for helium nuclei, only the TOF-triggered events were analyzed. The systematic error in the TOF trigger efficiency is negligibly small.
[b] Below 10 GeV nucleon$^{-1}$ quality check was not imposed.

data-taking time was measured exactly to be 33,370 s by counting 1 MHz clock pulses with a scaler system gated by a "ready" status that controls the first-level trigger. The resultant live-time ratio was as high as 86.4%.

The energy of each particle at the top of the atmosphere was calculated by summing up the ionization energy losses with tracing back the event trajectory.

In order to estimate the interaction loss probabilities inside the residual atmosphere and the BESS detector, Monte Carlo simulations were performed. The Monte Carlo code was developed to incorporate detailed descriptions of various interactions of helium nuclei into GEANT (Brun et al. 1994), where the cross sections and angular distributions of the nuclear interactions were evaluated by fitting energy-dependent empirical formulae (Bradt & Peters 1950) to experimental data (Bizard et al. 1977 and references therein; Abdurakhimov et al. 1981 and references therein; Gasparyan et al. 1982; Ableev et al. 1985 and references therein; Grebenjuk et al. 1989 and references therein; Glagolev et al. 1993 and references therein; Abdullin et al. 1994 and references therein). The electromagnetic processes, mainly due to $\delta$-rays, were also treated properly. They are more significant in helium nuclei interactions because cross sections in electromagnetic processes ($\sigma_{em}$) behave as $\sim Z^2$, whereas those in hadronic processes ($\sigma_{had}$) are approximately proportional to $(2Z)^{2/3}$. The systematic errors in the Monte Carlo simulation originate mainly in uncertainties of $\sigma_{had}$ and $\sigma_{em}$. We attributed relative errors of $\pm 5\%$ to $\sigma_{had}$ ($p + A$), $\pm 5\%$ to $\sigma_{em}(p + A)$, $\pm 15\%$ to $\sigma_{had}(He + A)$, $\pm 20\%$ to $\sigma_{em}(He + A)$, and $\pm 20\%$ to $\sigma_{had}(CNO + A)$, where $A$ is an atomic nucleus of the target material.

The probabilities that protons and helium nuclei can pass through the whole detector without interaction were evaluated by applying the same single-track selection to the Monte Carlo events. The Monte Carlo simulation of the BESS detector well reproduced the observed event profile. By comparing the observed and simulated parameters used in the single-track selection, i.e., the number of tracks inside the tracking volume and the number of hit counters in each layer of the TOF hodoscopes, it was concluded that a discrepancy between the observed and simulated event shapes was $\pm 1.9\%$ for protons and $\pm 4.1\%$ for helium nuclei. This discrepancy was included in a systematic error of the single-track efficiency. Another source of the systematic error in the Monte Carlo simulation was uncertainty of the material distribution inside the BESS spectrometer, which was estimated to be $\pm 10\%$. The resultant single-track efficiencies were $87.6\% \pm 2.3\%$ for protons and $74.5\% \pm 6.9\%$ for helium nuclei at 1 GeV nucleon$^{-1}$ and $79.7\% \pm 2.9\%$ and $64.6\% \pm 7.5\%$ at 100 GeV nucleon$^{-1}$.

According to similar Monte Carlo studies, probabilities for primary cosmic rays to penetrate the residual atmosphere of 5 g cm$^{-2}$ are $93.8\% \pm 0.7\%$ and $91.3\% \pm 2.0\%$ at 10 GeV nucleon$^{-1}$ for protons and helium nuclei, respectively, and almost constant over the entire energy range discussed here. The errors include the uncertainties of the $\sigma_{had}$'s mentioned before and the residual atmosphere depth, to which we attributed a relative error of $\pm 10\%$.

Atmospheric secondary protons were subtracted based on the calculation for the minimum solar activity epoch by Papini, Grimani, & Stephens (1996). A secondary-to-primary proton ratio is $3.5\% \pm 0.4\%$ at 1 GeV nucleon$^{-1}$ and $1.5\% \pm 0.2\%$ above 10 GeV nucleon$^{-1}$. Atmospheric secondary helium above 1 GeV nucleon$^{-1}$ is dominated by fragments of heavier cosmic-ray nuclei (mainly carbon and oxygen). The flux ratio of the atmospheric secondary helium to the primary carbon and oxygen was calculated to be 0.14 at a depth of 5 g cm$^{-2}$, based on the total inelastic cross sections of CNO+Air interactions and the helium multiplicity in $^{12}C + CNO$ interactions (Ahmad, Khan, & Hasan 1989). The total correction of atmospheric secondary helium due to all nuclei with $Z > 2$ was estimated to be $1.6\% \pm 0.5\%$ at 1 GeV nucleon$^{-1}$ and $2.1\% \pm 0.6\%$ at 10 GeV nucleon$^{-1}$.

TABLE 2

RESIDUAL AIR EFFECT (%)

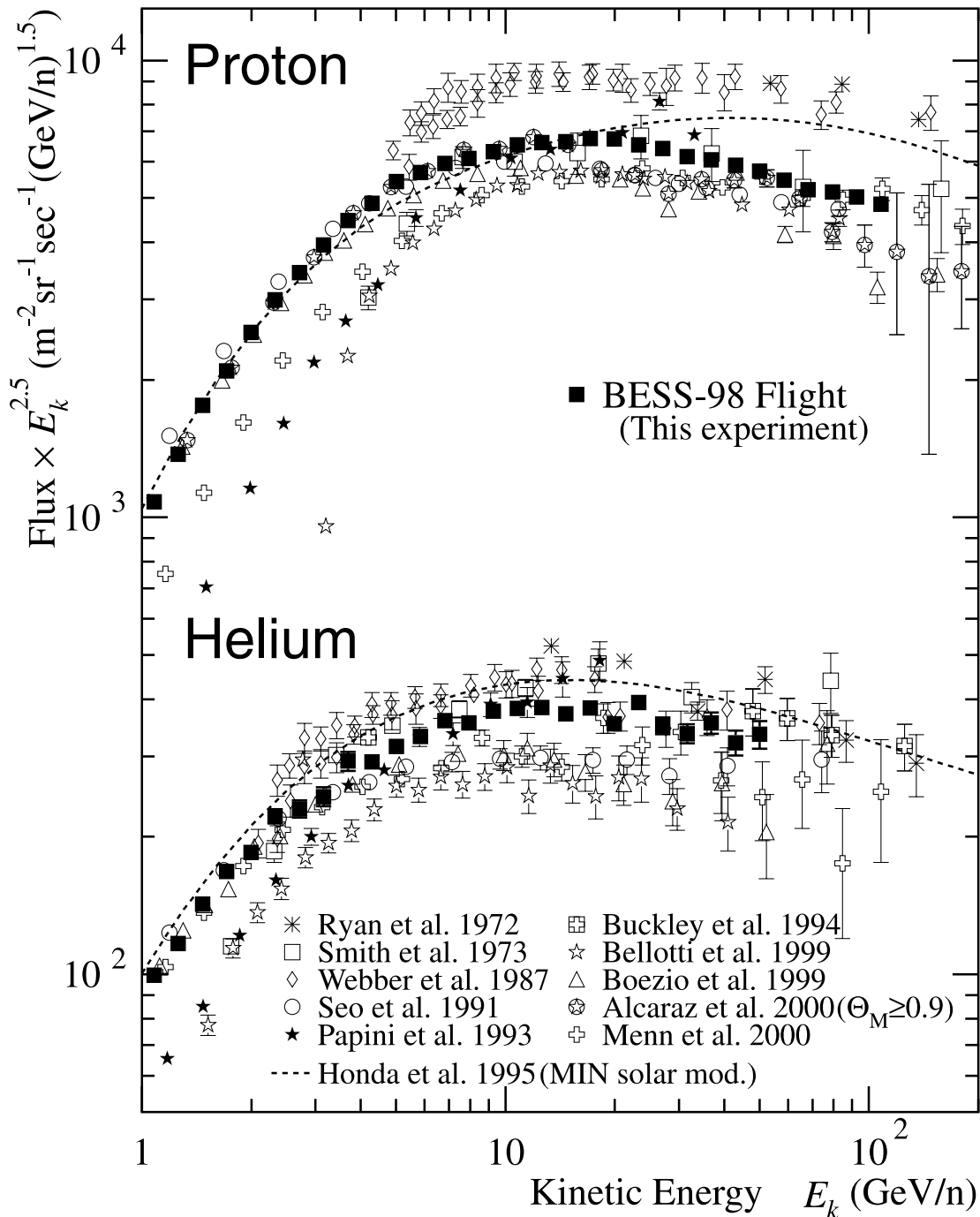| | PROTON KINETIC ENERGY (GeV nucleon$^{-1}$) | | | HELIUM KINETIC ENERGY (GeV nucleon$^{-1}$) | |
| --- | --- | --- | --- | --- | --- |
| AIR EFFECT | 1 | 10 | 100 | 1 | 10 |
| Survival probability .......... | $93.4 \pm 0.8$ | $93.8 \pm 0.7$ | $93.8 \pm 0.7$ | $91.5 \pm 3.1$ | $91.3 \pm 2.0$ |
| Secondary contribution...... | $3.5 \pm 0.4$ | $1.6 \pm 0.2$ | $1.5 \pm 0.2$ | $1.6 \pm 0.5$ | $2.1 \pm 0.6$ |

FIG. 4.—Absolute differential proton and helium spectra. Filled squares show results of the BESS-98 experiment. The spectra obtained by other experiments are also shown by different symbols indicated in the figure. Dashed lines show assumed spectra in one of the atmospheric neutrino flux calculations (Honda et al. 1995; M. Honda 1999, private communication).

In the estimations of the atmospheric secondary particle contributions, the errors were obtained by adding quadratically the uncertainties in the $\sigma_{had}$'s, the primary cosmic-ray fluxes, and the residual air depth. The $\sigma_{had}$'s were attributed the relative error of $\pm(5–20)\%$ depending on projectile particles, as has been mentioned before. We attributed relative errors of $\pm5\%$ to primary proton flux and $\pm20\%$ to primary heavier ($Z > 1$) cosmic-ray nuclei fluxes in the estimation of secondary particles. The residual air depth was estimated to have an error of $\pm10\%$ as mentioned before.

The combined systematic errors originating in the correction of the residual air effect were $\pm0.8\%$ for protons and $\pm3.1\%$ for helium nuclei at 1 GeV nucleon$^{-1}$ and $\pm0.7\%$ and $\pm2.1\%$ above 10 GeV nucleon$^{-1}$.

The efficiencies and the residual air effect are summarized in Tables 1 and 2, respectively.

## 4. SPECTRUM DEFORMATION EFFECT

Because of the finite resolution in rigidity measurement and the very steep spectral shape, the observed spectrum may suffer deformation. In a low-rigidity region well below the MDR, the spectrum deformation is negligibly small. In a higher rigidity region, however, a deflection becomes as small as an error in curvature measurement; thus, the spec-

TABLE 3

PROTON AND HELIUM FLUXES AT THE TOP OF THE ATMOSPHERE

| ENERGY RANGE (GeV nucleon$^{-1}$) | PROTON | | HELIUM | |
| | $\overline{E_k}$ (GeV nucleon$^{-1}$) | Flux $\pm \Delta\text{Flux}_{sta} \pm \Delta\text{Flux}_{sys}$ [(m$^2$ sr s GeV nucleon$^{-1}$)$^{-1}$] | $\overline{E_k}$ (GeV nucleon$^{-1}$) | Flux $\pm \Delta\text{Flux}_{sta} \pm \Delta\text{Flux}_{sys}$ [(m$^2$ sr s GeV nucleon$^{-1}$)$^{-1}$] |
|---|---|---|---|---|
| 1.00–1.17......... | 1.08 | $8.92 \pm 0.12 \pm 0.22 \times 10^2$ | 1.08 | $8.21 \pm 0.26 \pm 0.62 \times 10$ |
| 1.17–1.36......... | 1.26 | $7.72 \pm 0.11 \pm 0.19 \times 10^2$ | 1.26 | $6.57 \pm 0.22 \pm 0.50 \times 10$ |
| 1.36–1.58......... | 1.47 | $6.74 \pm 0.09 \pm 0.17 \times 10^2$ | 1.47 | $5.46 \pm 0.19 \pm 0.41 \times 10$ |
| 1.58–1.85......... | 1.71 | $5.46 \pm 0.08 \pm 0.14 \times 10^2$ | 1.71 | $4.38 \pm 0.15 \pm 0.33 \times 10$ |
| 1.85–2.15......... | 2.00 | $4.52 \pm 0.07 \pm 0.11 \times 10^2$ | 2.00 | $3.29 \pm 0.12 \pm 0.25 \times 10$ |
| 2.15–2.51......... | 2.33 | $3.63 \pm 0.05 \pm 0.09 \times 10^2$ | 2.33 | $2.69 \pm 0.10 \pm 0.21 \times 10$ |
| 2.51–2.93......... | 2.71 | $2.83 \pm 0.04 \pm 0.07 \times 10^2$ | 2.71 | $1.90 \pm 0.08 \pm 0.15 \times 10$ |
| 2.93–3.41......... | 3.16 | $2.22 \pm 0.04 \pm 0.06 \times 10^2$ | 3.15 | $1.38 \pm 0.07 \pm 0.11 \times 10$ |
| 3.41–3.98......... | 3.68 | $1.71 \pm 0.03 \pm 0.05 \times 10^2$ | 3.68 | $1.12 \pm 0.05 \pm 0.09 \times 10$ |
| 3.98–4.64 ........ | 4.30 | $1.27 \pm 0.02 \pm 0.03 \times 10^2$ | 4.30 | $7.62 \pm 0.09 \pm 0.63$ |
| 4.64–5.41......... | 5.01 | $9.65 \pm 0.19 \pm 0.26 \times 10$ | 5.01 | $5.60 \pm 0.07 \pm 0.46$ |
| 5.41–6.31 ........ | 5.84 | $6.89 \pm 0.15 \pm 0.19 \times 10$ | 5.84 | $4.02 \pm 0.05 \pm 0.33$ |
| 6.31–7.36......... | 6.81 | $4.91 \pm 0.02 \pm 0.20 \times 10$ | 6.80 | $2.96 \pm 0.04 \pm 0.24$ |
| 7.36–8.58......... | 7.94 | $3.43 \pm 0.01 \pm 0.14 \times 10$ | 7.92 | $1.99 \pm 0.03 \pm 0.16$ |
| 8.58–10.0......... | 9.25 | $2.42 \pm 0.01 \pm 0.10 \times 10$ | 9.24 | $1.44 \pm 0.03 \pm 0.12$ |
| 10.0–11.7......... | 10.8 | $1.70 \pm 0.01 \pm 0.07 \times 10$ | 10.8 | $9.98 \pm 0.20 \pm 0.81 \times 10^{-1}$ |
| 11.7–13.6......... | 12.6 | $1.18 \pm 0.01 \pm 0.05 \times 10$ | 12.6 | $6.82 \pm 0.15 \pm 0.55 \times 10^{-1}$ |
| 13.6–15.8......... | 14.6 | $8.05 \pm 0.04 \pm 0.33$ | 14.6 | $4.50 \pm 0.12 \pm 0.36 \times 10^{-1}$ |
| 15.8–18.5......... | 17.1 | $5.57 \pm 0.03 \pm 0.23$ | 17.1 | $3.16 \pm 0.09 \pm 0.26 \times 10^{-1}$ |
| 18.5–21.5......... | 19.9 | $3.78 \pm 0.03 \pm 0.16$ | 19.9 | $1.99 \pm 0.07 \pm 0.16 \times 10^{-1}$ |
| 21.5–25.1......... | 23.2 | $2.51 \pm 0.02 \pm 0.10$ | 23.2 | $1.51 \pm 0.05 \pm 0.12 \times 10^{-1}$ |
| 25.1–29.3......... | 27.1 | $1.67 \pm 0.01 \pm 0.07$ | 27.0 | $9.15 \pm 0.39 \pm 0.74 \times 10^{-2}$ |
| 29.3–34.1......... | 31.5 | $1.10 \pm 0.01 \pm 0.05$ | 31.5 | $5.98 \pm 0.29 \pm 0.49 \times 10^{-2}$ |
| 34.1–39.8......... | 36.8 | $7.35 \pm 0.08 \pm 0.31 \times 10^{-1}$ | 36.9 | $4.30 \pm 0.23 \pm 0.35 \times 10^{-2}$ |
| 39.8–46.4 ........ | 42.9 | $4.87 \pm 0.06 \pm 0.20 \times 10^{-1}$ | 42.9 | $2.65 \pm 0.17 \pm 0.22 \times 10^{-2}$ |
| 46.4–54.1......... | 50.0 | $3.22 \pm 0.05 \pm 0.14 \times 10^{-1}$ | 49.8 | $1.88 \pm 0.13 \pm 0.16 \times 10^{-2}$ |
| 54.1–63.1 ........ | 58.3 | $2.10 \pm 0.04 \pm 0.09 \times 10^{-1}$ | ... | ... |
| 63.1–73.6......... | 67.9 | $1.36 \pm 0.03 \pm 0.06 \times 10^{-1}$ | ... | ... |
| 73.6–85.8......... | 79.3 | $9.17 \pm 0.20 \pm 0.39 \times 10^{-2}$ | ... | ... |
| 85.8–100.......... | 92.6 | $6.08 \pm 0.15 \pm 0.26 \times 10^{-2}$ | ... | ... |
| 100.–117......... | 108. | $4.00 \pm 0.12 \pm 0.17 \times 10^{-2}$ | ... | ... |

trum deformation is to be considered. The effect of the finite resolution was estimated by simulation, where the error in rigidity measurement was tuned to reproduce the distribution shown in Figure 2. As for an input spectrum for the simulation, it was selected to follow the observed proton spectrum below ∼10 GV and gradually approach a power-law spectrum with increasing rigidity. The input spectrum was well described by the following empirical formula:

$$\frac{dN}{dR} \propto R^{-\gamma}\beta^{P_1} \exp\left(-\frac{P_2}{P_3 + R^{P_4}}\right), \quad (1)$$

where $\gamma$ is a spectral index and $P_1$–$P_4$ are fitting parameters. Three cases of spectral indices of 2.70, 2.75, and 2.80 were tested in these simulation studies. The deformation effect was found to be smaller than 1% below 25 GV, but it became visible with increasing rigidity. The simulated spectrum gradually got lower than the original spectrum with a ratio of −2.5% at 70 GV and then rapidly rose to ±0% at around 120 GV. At the MDR of 200 GV, the spectrum deformation effect reached about +10%. A dependence of the simulated spectrum on the three input spectra ($\gamma = 2.70$, 2.75, and 2.80) was smaller than ±1% below 25 GV and rapidly increased to ±5% at around 120 GV. The spectrum deformation effect is as small as the statistical errors over the energy range in this analysis. An approach to further correction of the spectrum deformation by using an unfolding method had been also evaluated as separately discussed in the Appendix.

## 5. EXPERIMENTAL RESULTS AND CONCLUSION

The proton and helium fluxes in the energy ranges of 1–120 GeV nucleon$^{-1}$ and 1–54 GeV nucleon$^{-1}$, respectively, at the top of the atmosphere have been obtained from the BESS-98 flight data as summarized in Table 3 and as shown in Figure 4 in comparison with other experiments (Ryan, Ormes, & Balasubrahmanyan 1972; Smith et al. 1973; Webber, Golden, & Stephens 1987; Seo et al. 1991; Papini et al. 1993; Buckley et al. 1994; Bellotti et al. 1999; Boezio et al. 1999; Alcaraz et al. 2000; Menn et al. 2000). The first and second errors in Table 3 represent statistical and systematic errors, respectively. The overall errors including both errors are less than ±5% for protons and ±10% for helium nuclei. The dotted lines in Figure 4 indicate the spectra assumed in one of the calculations of atmospheric neutrinos (Honda et al. 1995; M. Honda 1999, private communication).

Our results, as well as other recent measurements, are more favorable to lower fluxes than the ones assumed in the atmospheric neutrino calculation especially above a few tens of GeV nucleon$^{-1}$. It may suggest the importance of reconsideration for the atmospheric neutrino flux predictions. Precise measurements of primary cosmic rays will

help to improve the accuracy in the atmospheric neutrino calculations.

The authors thank NASA and NSBF for their cooperation to realize the successful balloon flight operation. This experiment was supported by Grants-in-Aid from Monbusho and Heiwa Nakajima Foundation in Japan and by

NASA in the USA. They deeply thank ISAS and KEK for their continuous support and encouragement for the BESS experiment. They would especially like to thank Professor T. Sumiyoshi and his group for their kind guidance and cooperation to develop the silica aerogel Cerenkov radiator for the flight in 1998. The analysis was performed with the computing facilities at ICEPP, the University of Tokyo.

## APPENDIX

### UNFOLDING THE MEASURED SPECTRA

The spectrum deformation due to the finite resolution in rigidity measurement could be corrected by a statistical procedure, such as an unfolding method based on Bayes's theorem (D'Agostini 1995). In the method, the finite resolution effect is described by a "smearing matrix," which was estimated from a simulation in consideration of the resolution function shown in Figure 2. In the beginning of the unfolding procedure, an "initial" spectrum has to be chosen. It will result in an unfolded spectrum by applying Bayes's theorem iteratively. The "initial" spectra were presumed in the same manner as equation (1). The spectral indices of 2.80 for protons and 2.70 for helium nuclei were chosen because the emulsion chamber experiments showed proton and helium spectra have spectral indices of $2.80 \pm 0.04$ and $2.68^{+0.04}_{-0.06}$, respectively, above a few tens of TeV (Asakimori et al. 1998). Figure 5 shows the results of the unfolding based on Bayes's theorem. The open squares and closed circles in Figure 5 show the measured and unfolded spectra, respectively. The dotted lines show "initial" spectra. The resultant unfolded spectrum was found to inherit characteristics of the "initial" spectrum in the shape of smooth curve. In order to estimate the dependence on the "initial" spectrum, another two "initial" spectra were examined with changing the spectral indices $\pm 0.05$. Deviations among the resultant unfolded spectra were $\pm 1\%$ below 120 GeV nucleon$^{-1}$ for protons and 60 GeV nucleon$^{-1}$ for helium nuclei and $\pm 3\%$ at 200 GeV nucleon$^{-1}$ for protons and 100 GeV nucleon$^{-1}$ for helium nuclei. And furthermore, the shape of the resultant unfolded spectrum was found to depend on the number of iterations. A repeat of unfolding could smear characteristics of the observed spectrum. The unfolded spectra shown in Figure 5 were obtained after the second iteration.

Figure 6 shows a degree of the spectrum deformation obtained by comparing the measured and unfolded spectra of protons. The estimation from the simulation described in § 4 is also indicated by closed circles. In the simulation estimation, the error in rigidity measurement was simulated following the distribution of the deflection resolution shown in Figure 2. In a
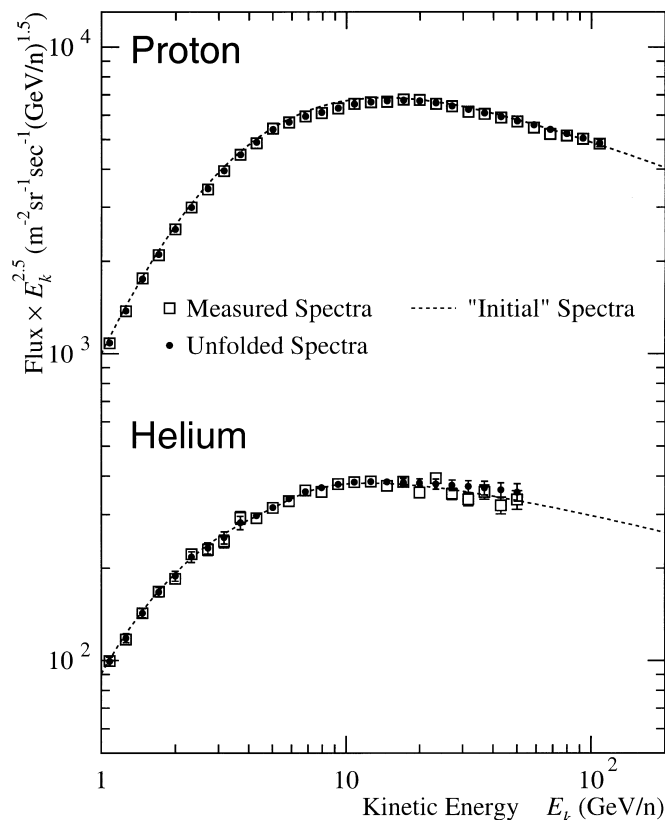


FIG. 5.—Unfolding of the measured differential proton and helium spectra. Open squares show the measured spectra obtained from the BESS-98 experiment. Dashed lines show "initial" spectra assumed in the unfolding procedure. Closed circles show the resultant unfolded spectra.
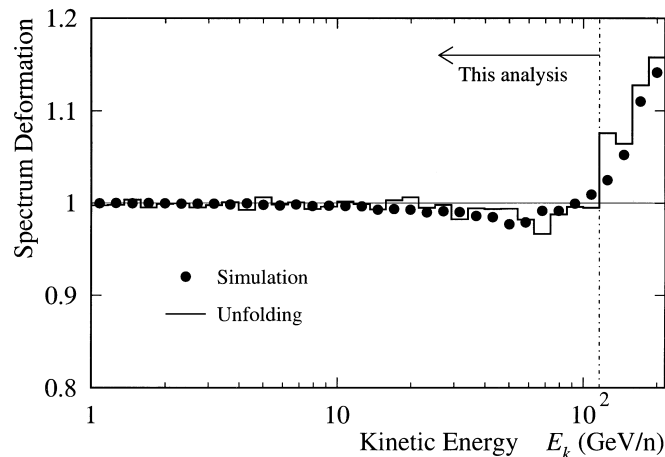
Fig. 6.—Spectrum deformation effect for protons. The histogram shows the ratio of the measured spectrum to the resultant unfolded spectrum. Closed circles show the estimation from the simulation. In both cases, the proton spectrum was assumed to gradually approach a power-law spectrum with a spectral index of 2.80.

higher energy region above 120 GeV nucleon$^{-1}$, as shown in Figure 6, the spectrum deformation effect rapidly increases; therefore, a large correction has to be applied to the measured spectrum. A large correction might cause more systematic errors. Below 120 GeV nucleon$^{-1}$ the spectrum deformation effect was estimated to be no more than $\pm 3\%$, which will not cause a major deformation of the spectrum.

In order to perform the unfolding, it is very important to start with a proper " initial " spectrum which is close enough to the " true " one. In the iterative procedure, measured data with a good statistics are also required for a good convergence. More precise measurement of spectra in wider energy ranges is essentially important and is planned to be carried out with upgrading the BESS spectrometer.

REFERENCES

Abdullin, S. K., et al. 1994, Nucl. Phys. A, 569, 753
Abdurakhimov, A. K., et al. 1981, Nucl. Phys. A, 362, 376
Ableev, V. G., et al. 1985, Acta Phys. Polonica B, 16, 913
Ahmad, M. S., Khan, M. Q. R., & Hasan, R. 1989, Nucl. Phys. A, 499, 821
Ajima, Y., et al. 2000, Nucl. Instr. Methods A, 443, 71
Alcaraz, J., et al. 2000, Phys. Lett. B, 472, 215
Allison, W. W. M., et al. 1999, Phys. Lett. B, 449, 137
Ambrosio, M., et al. 1998, Phys. Lett. B, 434, 451
Asakimori, K., et al. 1998, ApJ, 502, 278
Asaoka, Y., Abe, K., Yoshimura, K., Ishino, M., Fujikawa, M., & Orito, S. 1998, Nucl. Instr. Methods A, 416, 236
Bellotti, R., et al. 1999, Phys. Rev. D, 60, 052002
Bizard, G., et al. 1977, Nucl. Phys. A, 285, 461
Boezio, M., et al. 1999, ApJ, 518, 457
Bradt, H. L., & Peters, B. 1950, Phys. Rev., 77, 54
Brun, R., et al. 1994, GEANT, Detector Description and Simulation Tool, CERN Program Library (Geneva: CERN)
Buckley, J., Dwyer, J., Müller, D., Swordy, S., & Tang, K. K. 1994, ApJ, 429, 736
D'Agostini, G. 1995, Nucl. Instr. Methods A, 362, 487
Engelmann, J. J., et al. 1990, A&A, 233, 96
Fukuda, Y., et al. 1998, Phys. Rev. Lett., 81, 1562
Gasparyan, A. P., et al. 1982, Yad. Fiz., 36, 690
Glagolev, V. V., et al. 1993, Z. Phys. C, 60, 421
Grebenjuk, O. G., Khanzadeev, A. V., Korolev, G. A., Manayenkov, S. I., Saudinos, J., Velichko, G. N., & Vorobyav, A. A. 1989, Nucl. Phys. A, 500, 637

Honda, M., Kajita, T., Kasahara, K., & Midorikawa, S. 1995, Phys. Rev. D, 52, 4985
Karimäki, V. 1991, Nucl. Instr. Methods A, 305, 187
Menn, W., et al. 2000, ApJ, 533, 281
Orito, S. 1987, Proc. ASTROMAG Workshop, ed. J. Nishimura, K. Nakamura, & A. Yamamoto (Ibaraki: Natl. Lab. for High Energy Phys.), 111
Papini, P., et al. 1993, Proc. 23rd Int. Cosmic-Ray Conf. (Calgary), 1, 579
Papini, P., Grimani, C., & Stephens, S. A. 1996, Nuovo Cimento, 19C, 367
Ryan, M. J., Ormes, J. F., & Balasubrahmanyan, V. K. 1972, Phys. Rev. Lett., 28, 985
Seo, E. S., et al. 1997, Proc. 25th Int. Cosmic-Ray Conf. (Durban), 3, 373
Seo, E. S., Ormes, J. F., Streitmatter, R. E., Stochaj, S. J., Jones, W. V., & Stephens, S. A. 1991, ApJ, 378, 763
Shikaze, Y., et al. 2000, Nucl. Instr. Methods A, in press (hep-ex/0002047)
Smith, L. H., Buffington, A., Smoot, G. F., & Alvarez, L. W. 1973, ApJ, 180, 987
Sullivan, J. D. 1971, Nucl. Instr. Methods, 95, 5
Sumiyoshi, T., Adachi, I., Enomoto, R., Iijima, T., Suda, R., & Yokoyama, M. 1998, J. Noncryst. Solids, 225, 369
Webber, W. R., Golden, R. L., & Stephens, S. A. 1987, Proc. 20th Int. Cosmic-Ray Conf. (Moscow), 1, 325
Yamamoto, A., et al. 1994, Adv. Space Res., 14, 75